

**Paramagnetic rare-earth oxide Nd<sub>2</sub>O<sub>3</sub> investigated by muon spin spectroscopy**R. C. Vilão <sup>1,\*</sup>, M. A. Curado <sup>1,2</sup>, H. V. Alberto,<sup>1</sup> J. M. Gil <sup>1</sup>, J. A. Paixão,<sup>1</sup> J. S. Lord <sup>3</sup> and A. Weidinger<sup>4</sup><sup>1</sup>*CFisUC, Department of Physics, University of Coimbra, P-3004-516 Coimbra, Portugal*<sup>2</sup>*International Iberian Nanotechnology Laboratory, P-4715-330 Braga, Portugal*<sup>3</sup>*ISIS Facility, Rutherford Appleton Laboratory, Chilton, Didcot, Oxon OX11 0QX, United Kingdom*<sup>4</sup>*Helmholtz-Zentrum Berlin für Materialien und Energie, Institute for Nanospectroscopy, D-12489 Berlin, Germany*

(Received 3 September 2019; revised manuscript received 18 October 2019; published 12 November 2019)

In the context of a systematic study of oxide materials with the muon spin spectroscopy ( $\mu$ SR) technique, we report here on an investigation of paramagnetic Nd<sub>2</sub>O<sub>3</sub>. The question was whether the magnetism of Nd<sup>3+</sup> has an influence on the observed signals. In Nd<sub>2</sub>O<sub>3</sub>, as in the other oxides, a weakly paramagnetic component is observed besides the pure diamagnetic fraction. The paramagnetic part is assigned to a transient state formed between the initial atomic and the final bound muonium configuration. In addition, a fast relaxing signal ( $\lambda \sim 7 \mu\text{s}^{-1}$ ) with 10% to 20% fraction is seen in longitudinal field. Contrary to this general behavior of the oxide materials, in the present magnetic compound, a resonancelike structure is seen in the temperature range around 40 K. We assign it tentatively to a dynamical process related to the population of the first excited Kramers doublet of the Nd<sup>3+</sup> ion at 2.6 meV.

DOI: [10.1103/PhysRevB.100.205203](https://doi.org/10.1103/PhysRevB.100.205203)**I. INTRODUCTION**

Oxides with trivalent rare-earth cations, of the general sesquioxide form R<sub>2</sub>O<sub>3</sub>, play an important role in solid state physics and materials science and present a rich field for technological research and applications [1–6]. In fact, as rare-earth sesquioxides can present more than one crystal structure, for particular temperature and pressure conditions, they may exhibit several phases (spin, charge, orbital states), which can enhance the diversity in potential applications. Among rare-earth sesquioxides, Nd<sub>2</sub>O<sub>3</sub> assumes a prominent role in photonic applications, as a candidate high- $\kappa$  dielectric, in sensor or catalyst applications [7–13].

The hydrogen impurity is mostly unavoidable within materials and can have a deep impact in the properties of semiconductors and insulators, particularly in the electrical properties. Hydrogen is known to passivate impurities or defects in semiconductors, but isolated hydrogen can also act as a dopant or as compensating amphoteric impurity [14–16]. The knowledge of the isolated hydrogen configurations inside the material is of fundamental importance in order to understand the electrical properties [17–20].

Nd<sub>2</sub>O<sub>3</sub> is no exception and the growth methods for this rare-earth sesquioxide imply the possibility of introduction of the hydrogen impurity in high concentrations [11,21,22]. Thin films of Nd<sub>2</sub>O<sub>3</sub> grown by atomic layer deposition present hydrogen concentration as high as 1.2% [22]. However, little is known about the effect of hydrogen in Nd<sub>2</sub>O<sub>3</sub>.

The investigation of the configurations of isolated hydrogen in semiconductors and oxides has known an intensive contribution from the experimental results obtained by muon spin spectroscopy ( $\mu$ SR) on muonium [15,16,23–25]. This

atom formed by an electron bound to a positive muon can be thought of in condensed matter physics and chemistry as a light pseudoisotope of hydrogen, due to the similarity of its electronic properties [15,25,26]. The implantation of positive muons allows us to probe the ground state as well as transient metastable configurations of muonium, which allows us to clarify many microscopic aspects of the hydrogen dynamics inside the material [27–30].

Muon spectroscopy studies of muonium as a pseudoisotope of hydrogen are however generally undertaken in diamagnetic materials. The muon being a very sensitive magnetic probe, the existence of paramagnetism may impact on the  $\mu$ SR signal. The presence of the paramagnetic Nd<sup>3+</sup> ions in Nd<sub>2</sub>O<sub>3</sub> therefore brings the additional challenge of separating the effect of the paramagnetic ions on the usual signals of the different muonium configurations in this paramagnetic oxide.

In insulating and semiconducting oxides, two main signals are usually observed in  $\mu$ SR studies: (i) precession of the muon spin at the characteristic Larmor frequency of the bare muon, assigned to the diamagnetic fraction, and (ii) characteristic frequencies of neutral muonium in an atomic or bound configuration [29,31]. Recently, additional signals from transient muonium configurations were reported [32–34].

Previous works in oxides with paramagnetic ions have focused on the diamagnetic fraction attributed to bare  $\mu^+$  [35–40], seldom on paramagnetic configurations [41]. The present work represents a successful attempt to characterize muonium configurations in a paramagnetic oxide.

**II. EXPERIMENTAL DETAILS AND RESULTS**

A high-purity polycrystalline sample of Nd<sub>2</sub>O<sub>3</sub> was used (obtained commercially from Alfa Aesar, REacton, 99.999%) in this work. Nd<sub>2</sub>O<sub>3</sub> crystallizes in the hexagonal La<sub>2</sub>O<sub>3</sub> structure (A-type, space-group  $P\bar{3}m1$ , No. 164) [42].

\*ruivilao@uc.pt

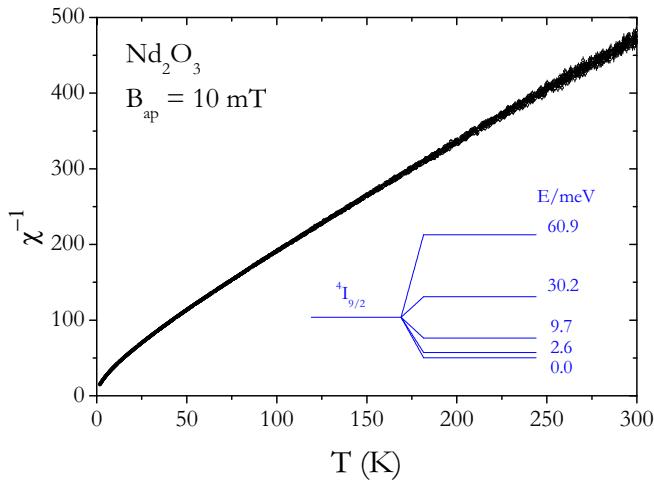


FIG. 1. Temperature dependence of the inverse magnetic volume susceptibility (in the SI system) of  $\text{Nd}_2\text{O}_3$ , for an external applied magnetic field  $B_{\text{ap}} = 10$  mT. The inset shows the well-known lifting of the degeneracy of the tenfold  $^4I_{9/2}$  ground state of the  $\text{Nd}^{3+}$  paramagnetic ion due to the effect of the crystal field.

Conventional magnetometry measurements were undertaken at the TAIL Facility of the University of Coimbra: the temperature dependent inverse magnetic susceptibility of our sample (subject to an external magnetic field  $B = 10$  mT) is shown in Fig. 1 in the temperature interval 1.8 to 300 K. Long-range antiferromagnetic order in  $\text{Nd}_2\text{O}_3$  sets in only for temperatures below 550 mK [13]. The temperature dependence of the susceptibility at high temperatures is well described by a Curie-Weiss model with the expected magnetic moment for the  $\text{Nd}^{3+}$  ion. The deviation at low temperatures is a well-known crystal field effect associated with the lift up of the degeneracy of the  $J = 9/2$  ground state multiplet [43]. The corresponding energy levels are shown as an inset in Fig. 1 [44].

Muon spin spectroscopy experiments were performed at the EMU instrument of the ISIS Facility at the Rutherford-Appleton Laboratory (United Kingdom). Conventional muon spin rotation measurements were undertaken from  $T = 8$  K up to  $T = 640$  K with an applied transverse magnetic field  $B = 10$  mT. Longitudinal field measurements were also performed at room temperature. Calibration of the maximum asymmetry of the instrument was obtained using a silver sample. The analysis of the raw spectra was performed with the WiMDA software [45].

### A. $\mu\text{SR}$ time spectra

Figure 2 shows the experimental  $\mu\text{SR}$  time spectrum at low transverse field (10 mT) at the temperature of 100 K. The oscillation frequency corresponds to the Larmor precession frequency expected for the diamagnetic (bare) muon. However, the spectrum shows clearly two components, distinguished by the relaxation rate. The slow component (red line in the upper frame of Fig. 2) relaxes with a rate of  $\lambda = 0.05(1) \mu\text{s}^{-1}$  (due to nuclear moments) and is assigned to muons in a diamagnetic environment. Using an exponential rather than a Gaussian relaxation for the diamagnetic

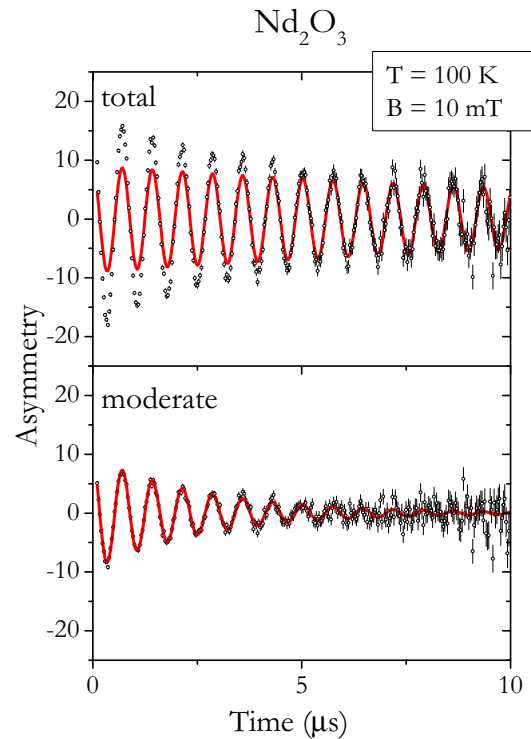


FIG. 2. Transverse field time spectrum at  $T = 100$  K and  $B = 10$  mT. Two relaxations can be distinguished: Slow [ $0.05(1) \mu\text{s}^{-1}$ ] and moderate [ $0.38(3) \mu\text{s}^{-1}$ ]. The total asymmetry is shown in the upper panel, together with the fitted slow relaxing component (red line). The lower panel displays the data after subtracting the slow component (red line in the upper panel), together with the fitted moderately relaxing component (red line in the lower panel).

component is justified since the nuclear spins of  $\text{Nd}_2\text{O}_3$  are diluted (the abundance of Nd isotopes with nuclear spins is 20.5%) and, in this situation, the internal field distribution from the nuclear magnetic moments is more Lorentzian than Gaussian like.

The difference between the total spectrum and the diamagnetic component is displayed in the lower frame of Fig. 2. The relaxation rate of this curve [ $\lambda = 0.38(3) \mu\text{s}^{-1}$ ] indicates that an interaction with an unpaired electron is involved. Similar signals were observed in many other systems [38,46–52]. We assign this moderately relaxing signal (moderate to distinguish it from fast, see fast signal in Fig. 3) to a transition state which is formed as an intermediate configuration between incoming atomic muonium and the final bound configuration (for details see Ref. [32]). The suggested underlying process is that the originally tightly bound electron of atomic muonium leaves the confinement at an interstitial site and forms a weakly bound configuration with an extended wave function similar to that of shallow donors in semiconductors. In this situation the hyperfine interaction is weak and probably fluctuating. The resulting average hyperfine interaction leads to line broadening around the diamagnetic line and thus to a relaxation of the diamagneticlike signal.

This assignment is controversial in the  $\mu\text{SR}$  community. In a number of papers the relaxing signal has been assigned to stopped  $\mu^+$  which after some delay captures an electron

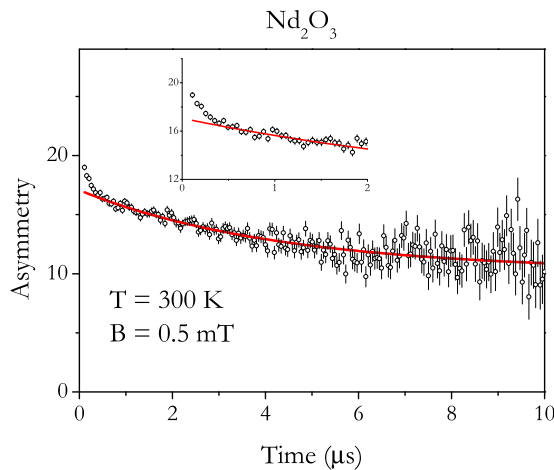


FIG. 3. Longitudinal field time spectrum at  $T = 300$  K and  $B = 0.5$  mT. The long-time behavior is fitted with a weakly relaxing function (red solid line) to allow an extrapolation to early times. The inset shows the first  $2 \mu\text{s}$  of the spectrum.

from the ionization track of the implanted muon [47,50,53]. Assignments to  $\text{Mu}^-$  have also been proposed [54]. These models were developed taking into account that the frequency of the signal is seemingly diamagnetic. We should, however, note that in a Mg-doped zirconia sample an upward shift of the frequency is seen for low external fields [32]. Similar upward shifts were observed also in other experiments [50,52]. This shift indicates the presence of a hyperfine interaction during the lifetime of the state and thus contradicts the model of a diamagnetic state with delayed capture or loss of an electron. The present experiment is not suited to observe this frequency shift—it requires adequate experimental conditions—but the similarity of the samples in the present and in these other experiments, as well as the similarity of the experimental results, justifies the application of the transition state model also in the case of  $\text{Nd}_2\text{O}_3$ .

We have also measured a longitudinal field decoupling curve at 300 K. A low-field time spectrum is shown in Fig. 3. The longtime behavior is fitted with a weakly relaxing function (red solid line) to allow an extrapolation to early times. The main emphasis in connection with Fig. 3 lies on the fast signal ( $\lambda \sim 7 \mu\text{s}^{-1}$ ) which is displayed separately in the inset of the figure. The amplitude ( $\sim 20\%$  fraction) and the relaxation are fairly constant up to longitudinal fields well above 100 mT. This indicates that a fairly large hyperfine interaction in the order of atomic muonium is involved. We assign the fast signal to delayed conversion of the incoming (excited) muonium to ground state muonium, possibly via a diamagneticlike transition state [32]. The fast signal is, due to dephasing, not seen in the transverse field experiment and constitutes the major part of the missing fraction in Figs. 2 and 4.

### B. Temperature dependence

In order to obtain an overview of the data we analyzed the transverse field measurement with a single frequency without distinguishing between the moderately and slowly relaxing

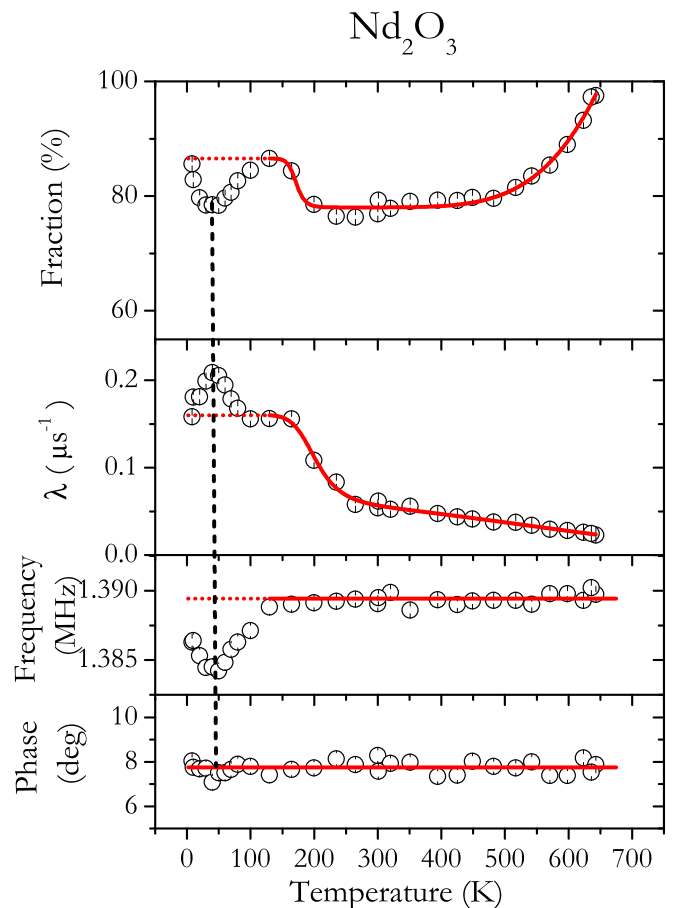


FIG. 4. Diamagneticlike component at a transverse magnetic field of  $B = 10$  mT: Fraction, relaxation ( $\lambda$ ), frequency, and phase from one-component analysis. The red lines mark the overall behavior of the parameters without the resonancelike feature at about 40 K.

signal. The fit parameters (fraction, relaxation rate, frequency, and phase) are displayed in Fig. 4.

A remarkable feature of the data is the resonancelike behavior at about 40 K. We discuss this part separately below. The rest of the data, indicated by the red lines, show a behavior similar to other oxides [33,49,51,55]. The fraction amounts to about 80% of all muons for the major part of the temperature range. At the highest temperatures above 500 K full recovery sets in. Below 200 K, the fraction increases by about 10%. The slightly higher fraction at low temperatures is attributed to a thermal spike effect described in a recent paper [34].

The relaxation rate shows a strong decrease in the temperature range between 150 and 250 K. This decrease is attributed to the delayed conversion of the paramagnetic to the diamagnetic configuration. The frequency and phase are fairly constant outside the resonance region and correspond to the values of the calibration measurement. The phase shows little or no resonance effect within experimental error.

Thus, three special phenomena are observed and will be discussed below. These are:

- (1) Recovery of the diamagnetic fraction above 500 K.
- (2) Conversion from paramagnetic to diamagnetic configuration around 200 K.
- (3) Resonancelike behavior at 40 K.

### III. DISCUSSION

The  $\mu$ SR signal of this experiment is basically diamagnetic, i.e., the precession frequency corresponds approximately to the Larmor frequency of the muon spin. However, the relaxation at low temperatures ( $\sim 0.38 \mu\text{s}^{-1}$ ) is larger than expected for the bare muon ( $\sim 0.05 \mu\text{s}^{-1}$ ), indicating an interaction with an unpaired electron. The larger relaxation disappears around 200 K due to the loss of the paramagnetic electron (ionization).

#### A. Full recovery of the diamagnetic fraction above 500 K

The increase of the fraction above 500 K is attributed to ionization of the missing fraction part. The activation energy amounts to 0.4(1) eV. This recovery is usually assigned to the thermal ionization of ground state muonium. However, this is not completely unambiguous. It is also possible that ionization takes place from some excited configuration before the ground state is formed. Then the 0.4 eV represents only a lower limit of the ionization energy of ground state muonium.

#### B. Conversion from paramagnetic to diamagnetic around 200 K

We assume that the strong change of the relaxation in Fig. 4 between 150 and 250 K is due to the delayed conversion of the weakly paramagnetic to the diamagnetic configuration. Thus, for an individual muon the spin precession relaxes first with the rate  $\lambda_e + \lambda_n$  and after some time with the rate  $\lambda_n$ . The rate  $\lambda_e$  is due to the interaction of the muon spin with the paramagnetic electron and  $\lambda_n$  to the interaction with nuclear spins. In the paramagnetic configuration both interactions are present, thus the sum of the two relaxation rates has to be taken. We assume that the muonium electron is strongly coupled to the Nd ions and takes part in the fast fluctuation of the Nd magnetic moments. As a result, an average hyperfine field is seen at the muon site. The average field from the electronic surrounding and the field from the nuclear moments are superimposed. Thus, the two relaxation rates  $\lambda_e$  and  $\lambda_n$  have to be added.

The ensemble averaging over all conversions with a mean conversion time  $\tau$  yields for the polarization function:

$$P(t) = a_1 \left( 1 - \frac{1}{\lambda_e \tau + 1} \right) \times \exp \left[ - \left( \lambda_e + \lambda_n + \frac{1}{\tau} \right) t \right] \cos(\omega t) + a_1 \frac{1}{\lambda_e \tau + 1} \exp(-\lambda_n t) \cos(\omega t), \quad (1)$$

$a_1$  is the fraction taking part in the conversion.  $P(t)$  has the form (without the cos term):

$$P(t) = f_{\text{para}} \exp \left[ - \left( \lambda_e + \lambda_n + \frac{1}{\tau} \right) t \right] + f_{\text{dia}} \exp(-\lambda_n t). \quad (2)$$

The relaxation of the paramagnetic fraction contains the contribution  $1/\tau$  from conversion.

The  $\mu$ SR time spectra were fitted with Eq. (1), assuming  $\lambda_n = 0.05(1) \mu\text{s}^{-1}$ , the value obtained by the fit of the

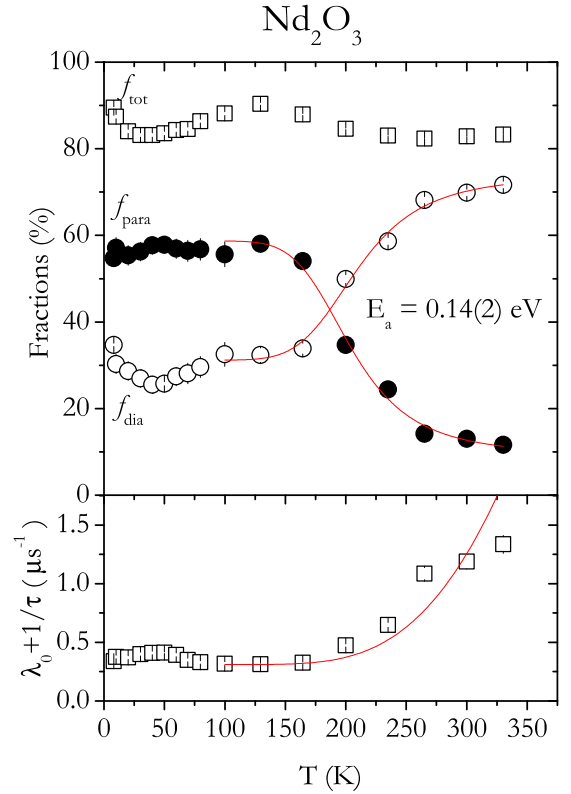


FIG. 5. Temperature dependence of the fractions  $f_{\text{dia}}$ ,  $f_{\text{para}}$ , and  $f_{\text{tot}} = f_{\text{dia}} + f_{\text{para}}$ , highlighting the conversion of the paramagnetic to diamagnetic fraction in the temperature region around 150 to 250 K. The fractions are shown in the upper frame and the relaxation rate of the moderately relaxing signal is shown in the lower frame. The relaxation of this component is caused by a distribution of internal fields ( $\lambda_0 = \lambda_e + \lambda_n$ ) and the contribution  $1/\tau$  from lifetime broadening. The fit curves correspond to an activation energy of 0.14(2) eV.

spectrum in Fig. 2, and treating  $a_1$ ,  $\lambda_e$ , and  $\tau$  as free parameters. In the transition region around 200 K,  $\lambda_e$  was fixed to the value obtained at lower temperatures to avoid ambiguities. Figure 5 shows in the upper frame the fractions  $f_{\text{para}}$ ,  $f_{\text{dia}}$ , and  $f_{\text{tot}} = f_{\text{para}} + f_{\text{dia}}$  as a function of temperature. In the lower frame the relaxation rate of the moderately relaxing paramagnetic signal is displayed. This relaxation has two contributions, one ( $\lambda_0 = \lambda_e + \lambda_n$ ) caused by the distribution of internal fields and the other ( $1/\tau$ ) caused by lifetime broadening.

In this analysis the decrease of the paramagnetic fraction equals the increase of the diamagnetic fraction. In the conversion region, the relaxation rate of the paramagnetic signal increases due to lifetime broadening. Thus the disappearance of the paramagnetic signal has two reasons, the decrease of the fraction and the increase of the relaxation rate. The two phenomena are correlated via the mean conversion time  $\tau$ . In the past, the separation of these phenomena posed problems and often either the fraction [56] or the relaxation [51] was kept constant and only the other parameter was varied. The correlated approach used here gives a more adequate description of the conversion process.

We assumed in the above analysis that the diamagnetic fraction is completely due to the delayed conversion

(ionization) of the paramagnetic configuration. However, part of the diamagnetic fraction may be formed promptly or at least on a different timescale than the diamagnetic fraction resulting from conversion. In the above analysis we did not distinguish between these two contributions.

### C. Resonance at 40 K

As seen in Fig. 4, a resonancelike structure shows up at around 40 K: the relaxation rate is increased and the fraction and frequency are decreased, the phase is little affected. This experimental feature (peaklike and diplike behavior) is indicative of a spin-lattice ( $T_1$ ) resonance effect. The present transverse field geometry is not well suited to measure  $T_1$  processes. However, in case of strong coupling of the muon spin with the surrounding electronic system,  $T_1$  relaxation may give rise to the observed effects. We assume for the analysis that a fluctuating spin-lattice interaction comes into resonance with the Larmor precession of the muon spin. Then the  $1/T_1$  relaxation rate has the following dependence:

$$\frac{1}{T_1(\mu)} \propto \frac{\tau_c}{1 + (\omega_L \tau_c)^2}, \quad (3)$$

with  $\omega_L = \gamma_\mu B_{\text{ext}}$  and  $\tau_c$  the correlation time. This yields at the peak position:

$$\begin{aligned} \omega_L \tau_c(T = 40 \text{ K}) &= 1 \\ \Rightarrow \tau_c(T = 40 \text{ K}) &= \frac{1}{\gamma_\mu B_{\text{ext}}} = 0.74 \mu\text{s}. \end{aligned} \quad (4)$$

Thus, a fairly slow dynamical process is involved which certainly does not correspond to the thermal fluctuation of the Nd moments. However, the low-lying Nd<sup>3+</sup> spin states are grouped in Kramers doublets and the first excited doublet lies only 2.6 meV above the ground state [44] and thus becomes appreciably populated at 40 K. Since the effective magnetic moments of the ground and excited state are different one obtains a fluctuating hyperfine interaction which may cause the  $T_1$  relaxation of the muon spin. In this interpretation, the resonance at 40 K in the present experiment is attributed to the excitation and deexcitation of the Nd<sup>3+</sup> first excited Kramers doublet with a rate in the order of  $1/(0.74 \mu\text{s})$  at 40 K.

Another dynamical process is the site change of the weakly bound electron with respect to the muon position. This will lead to a fluctuating hyperfine interaction with different values and orientations and could give rise to a  $T_1$  resonance in both magnetic and nonmagnetic materials. The fact that no such resonance has been observed so far in the nonmagnetic oxides points in the direction that the magnetism of Nd<sup>3+</sup>, in particular the excitation of the 2.6 meV Kramers doublet, plays a role. A combination of site changes and different occupations of the Nd<sup>3+</sup> spin states could also be responsible

for the resonance besides the fluctuation of the occupation. Thus, dynamical processes related to the occupation of the first excited Kramers doublet of Nd<sup>3+</sup> are the most likely interpretation of the resonance.

## IV. CONCLUSIONS

The  $\mu\text{SR}$  results for the present paramagnetic Nd<sub>2</sub>O<sub>3</sub> sample are qualitatively similar to data obtained for previously studied nonmagnetic oxides [31,34,49,51,55]. The main component (in the present experiment 80% to 90% fraction) is a signal with a diamagneticlike precession frequency but showing two different relaxations (moderate and slow). The moderately relaxing signal (sometimes called fast relaxing) [32,34,49] was heavily disputed in the past, assigned either to Mu<sup>+</sup> or Mu<sup>-</sup> with delayed capture or loss of an electron. In a recent paper [32] we gave a different interpretation of this state, i.e., assigned it to a weakly paramagnetic configuration which is formed as an intermediate state between compact muonium and the final bound configuration where the muon is incorporated in the lattice structure. The present data are fully consistent with this transition state interpretation.

For the conversion of the moderate to slow fraction around 200 K a new formalism was developed which avoids ambiguities between fraction and relaxation in the transition region. In this analysis, the fraction and the relaxation are determined by a single parameter, the mean lifetime  $\tau$ .

The present study on a paramagnetic sample reveals a resonancelike structure (the 40 K resonance), a feature not observed in previous experiments on nonmagnetic oxides [31,34,49,51,55]. We assign this resonance behavior tentatively to the excitation of the first Kramers doublet of Nd<sup>3+</sup> at 2.6 meV [44,57,58]. At 40 K, the ground and excited state are almost equally occupied but their population fluctuates. If this dynamical process comes into resonance with the muon Larmor precession, a spin-lattice relaxation may give rise to a resonance behavior. A combination of electron site changes and different occupations of the Nd<sup>3+</sup> spin states could also give rise to a fluctuating interaction. The present tentative assignment has to be checked by further experiments.

## ACKNOWLEDGMENTS

Access to the ISIS beam, through experiment RB1210309 [59], and the support of the ISIS muon team are gratefully acknowledged, as well as access to the TAIL-UC facility funded under QREN-Mais Centro project ICT\_2009\_02\_012\_1890. This work was supported with funds from FEDER (Programa Operacional Factores de Competitividade COMPETE) and from FCT—Fundação para a Ciência e Tecnologia (Portugal) under projects UID/FIS/04564/2016 and PTDC/FIS-MAC/29696/2017.

- [1] G.-Y. Adachi, and N. Imanaka, The binary rare earth oxides, *Chem. Rev.* **98**, 1479 (1998).
- [2] G. Adachi, N. Imanaka, and Z. C. Kang, *Binary Rare Earth Oxides* (Kluwer Academic, Dordrecht, 2004), Chap. 9.
- [3] R. Gillen and J. Robertson, Electronic structure of lanthanide oxide high K gate oxides, *Microelectron. Eng.* **109**, 72 (2013).

- [4] G. Azimi, D. Dhiman, H.-M. Kwon, A. T. Paxson, and K. K. Varanasi, Hydrophobicity of rare-earth oxide ceramic, *Nat. Mater.* **12**, 315 (2013).
- [5] E. Hemmer, N. Venkatachalam, H. Hyodo, A. Hattori, Y. Ebina, H. Kishimoto, and K. Soga, Upconverting and NIR emitting rare earth based nanostructures for NIR-bioimaging, *Nanoscale* **5**, 11339 (2013).

- [6] K. H. Goh, A. S. M. A. Haseeb, and Y. H. Wong, Lanthanide rare earth oxide thin film as an alternative gate oxide, *Mater. Sci. Semicond. Process.* **68**, 302 (2017).
- [7] A. A. Dakhel, Characterisation of Nd<sub>2</sub>O<sub>3</sub> thick gate dielectric for silicon, *Phys. Status Solidi (a)* **201**, 745 (2004).
- [8] C. R. Michel, A. H. Martínez-Preciado, and N. L. López Contreras, Gas sensing properties of Nd<sub>2</sub>O<sub>3</sub> nanostructured microspheres, *Sensors Actuators B* **184**, 8 (2013).
- [9] R. Yuvakkumar and S. I. Hong, Nd<sub>2</sub>O<sub>3</sub>: Novel synthesis and characterization, *J. Sol-Gel Sci. Technol.* **73**, 511 (2015).
- [10] A. Ramli, A. H. Shaari, H. Baqiah, H. B.C. S. Kean, M. M. A. Kechik, and Z. A. Talib, Role of Nd<sub>2</sub>O<sub>3</sub> nanoparticles addition on microstructural and superconducting properties of YBa<sub>2</sub>Cu<sub>3</sub>O<sub>7- $\delta$</sub>  ceramics, *J. Rare Earths* **34**, 895 (2016).
- [11] S. H. Jeon, K. Nam, H. J. Yoon, Y.-I. Kim, D. W. Cho, and Y. Sohn, Hydrothermal synthesis of Nd<sub>2</sub>O<sub>3</sub> nanorods, *Ceram. Int.* **43**, 1193 (2017).
- [12] S. Zinatloo-Ajabshir, S. Mortazavi-Derazkola, and M. Salavati-Niasari, Nd<sub>2</sub>O<sub>3</sub>-SiO<sub>2</sub> nanocomposites: A simple sonochemical preparation, characterization and photocatalytic activity, *Ultrason. Sonochem.* **42**, 171 (2018).
- [13] G. Sala, M. B. Stone, B. K. Rai, A. F. May, C. R. Dela Cruz, H. Suriya Arachchige, G. Ehlers, V. R. Fanelli, V. O. Garlea, M. D. Lumsden, D. Mandrus, and A. D. Christianson, Physical properties of the trigonal binary compound Nd<sub>2</sub>O<sub>3</sub>, *Phys. Rev. Mater.* **2**, 114407 (2018).
- [14] S. F. J. Cox, J. L. Gavartin, J. S. Lord, S. P. Cottrell, J. M. Gil, H. V. Alberto, J. Pirotto Duarte, R. C. Vilão, N. Ayres de Campos, D. J. Keeble, E. A. Davis, M. Charlton, and D. P. van der Werf, Oxide muonics: II. Modelling the electrical activity of hydrogen in wide-gap and high-permittivity dielectrics, *J. Phys.: Condens. Matter* **18**, 1079 (2006).
- [15] S. F. J. Cox, Muonium as a model for interstitial hydrogen in the semiconducting and semimetallic elements, *Rep. Prog. Phys.* **72**, 116501 (2009).
- [16] S. F. J. Cox, R. L. Lichti, J. S. Lord, E. A. Davis, R. C. Vilão, J. M. Gil, T. D. Veal, and Y. G. Celebi, The first 25 years of semiconductor muonics at ISIS, modelling the electrical activity of hydrogen in inorganic semiconductors and high- $\kappa$  dielectrics, *Phys. Scr.* **88**, 068503 (2013).
- [17] A. Weidinger, J. M. Gil, H. V. Alberto, R. C. Vilão, J. Pirotto Duarte, N. Ayres de Campos, and S. F. J. Cox, Shallow donor versus deep acceptor state in II-VI semiconductor compounds, *Physica B: Condens. Matter* **326**, 124 (2003).
- [18] R. L. Lichti, K. H. Chow, J. M. Gil, D. L. Stripe, R. C. Vilão, and S. F. J. Cox, Location of the H [+/-] level: Experimental limits for muonium, *Physica B* **376-377**, 587 (2006).
- [19] H. Okabe, M. Hiraishi, S. Takeshita, A. Koda, K. M. Kojima, and R. Kadono, Local electronic structure of interstitial hydrogen in iron disulfide, *Phys. Rev. B* **98**, 075210 (2018).
- [20] K. M. Kojima, M. Hiraishi, H. Okabe, A. Koda, R. Kadono, K. Ide, S. Matsuishi, H. Kumomi, T. Kamiya, and H. Hosono, Electronic structure of interstitial hydrogen in In-Ga-Zn-O semiconductor simulated by muon, *Appl. Phys. Lett.* **115**, 122104 (2019).
- [21] T. Liu, Y. Zhang, H. Li, and X. Shao, Synthesis and characteristics of Sm<sub>2</sub>O<sub>3</sub> and Nd<sub>2</sub>O<sub>3</sub> nanoparticles, *Langmuir* **19**, 7569 (2003).
- [22] J. Päiväsäari, M. Putkonen, and L. Niinistö, A comparative study on lanthanide oxide thin films grown by atomic layer deposition, *Thin Solid Film* **472**, 275 (2005).
- [23] R. C. Vilão, J. M. Gil, A. Weidinger, H. V. Alberto, J. Pirotto Duarte, N. Ayres de Campos, R. L. Lichti, K. H. Chow, and S. F. J. Cox, Information on hydrogen states in II-VI semiconductor compounds from a study of their muonium analogues, *Nucl. Instrum. Methods Phys. Res. Sect. A* **580**, 438 (2007).
- [24] K. Shimomura and T. U. Ito, Electronic structure of hydrogen donors in semiconductors and insulators probed by muon spin rotation, *J. Phys. Soc. Jpn.* **85**, 091013 (2016).
- [25] P. W. Mengyan, The role of muons in semiconductor research, in *Characterisation and Control of Defects in Semiconductors*, edited by F. Tuomisto (IET, London, 2019).
- [26] R. C. Vilão, R. B. L. Vieira, H. V. Alberto, J. M. Gil, A. Weidinger, R. L. Lichti, B. B. Baker, P. W. Mengyan, and J. S. Lord, Muonium donor in rutile TiO<sub>2</sub> and comparison with hydrogen, *Phys. Rev. B* **92**, 081202(R) (2015).
- [27] A. G. Marinopoulos, Incorporation and migration of hydrogen in yttria-stabilized cubic zirconia: Insights from semilocal and hybrid-functional calculations, *Phys. Rev. B* **86**, 155144 (2012).
- [28] A. G. Marinopoulos, Protons in cubic yttria-stabilized zirconia: Binding sites and migration pathways, *Solid State Ionics* **315**, 116 (2017).
- [29] A. G. Marinopoulos, R. C. Vilão, H. V. Vieira, H. V. Alberto, J. M. Gil, M. V. Yakushev, R. Scheuermann, and T. Goko, Defect levels and hyperfine constants of hydrogen in beryllium oxide from hybrid-functional calculations and muonium spectroscopy, *Philos. Mag.* **97**, 2108 (2017).
- [30] A. G. Marinopoulos, R. C. Vilão, H. V. Alberto, and J. M. Gil, Electronic structure and migration of interstitial hydrogen in the rutile phase of TiO<sub>2</sub>, *J. Phys.: Condens. Matter* **30**, 425503 (2018).
- [31] E. L. da Silva, A. G. Marinopoulos, R. B. L. Vieira, R. C. Vilão, H. V. Alberto, J. M. Gil, R. L. Lichti, P. W. Mengyan, and B. B. Baker, Electronic structure of interstitial hydrogen in lutetium oxide from DFT+*U* calculations and comparison study with  $\mu$ SR spectroscopy, *Phys. Rev. B* **94**, 014104 (2016).
- [32] R. C. Vilão, R. B. L. Vieira, H. V. Alberto, J. M. Gil, and A. Weidinger, Role of the transition state in muon implantation, *Phys. Rev. B* **96**, 195205 (2017).
- [33] R. C. Vilão, R. B. L. Vieira, H. V. Alberto, J. M. Gil, A. Weidinger, R. L. Lichti, P. W. Mengyan, B. Baker, and J. S. Lord, Barrier model in muon implantation and application to Lu<sub>2</sub>O<sub>3</sub>, *Phys. Rev. B* **98**, 115201 (2018).
- [34] R. C. Vilão, H. V. Alberto, J. M. Gil, and A. Weidinger, Thermal spike in muon implantation, *Phys. Rev. B* **99**, 195206 (2019).
- [35] E. Holzschuh, A. B. Denison, W. Kündig, P. F. Meier, and B. D. Patterson, Muon-spin-rotation experiments in orthoferri-tes, *Phys. Rev. B* **27**, 5294 (1983).
- [36] T. Lancaster, S. J. Blundell, F. L. Pratt, C. H. Gardiner, W. Hayes, and A. T. Boothroyd, A  $\mu^+$ SR study of the rare earth antiferromagnet PrO<sub>2</sub>, *J. Phys.: Condens. Matter* **15**, 8407 (2003).
- [37] R. M. D'Ortenzio, H. A. Dabkowska, S. R. Dunsiger, B. D. Gaulin, M. J. P. Gingras, T. Goko, J. B. Kycia, L. Liu, T. Medina, T. J. Munsie, D. Pomaranski, K. A. Ross, Y. J. Uemura, T. J. Williams, and G. M. Luke, Unconventional magnetic ground state in Yb<sub>2</sub>Ti<sub>2</sub>O<sub>7</sub>, *Phys. Rev. B* **88**, 134428 (2013).

- [38] J. A. Rodriguez, A. Yaouanc, B. Barbara, E. Pomjakushina, P. Quémerais, and Z. Salman, Muon diffusion and electronic magnetism in Y<sub>2</sub>Ti<sub>2</sub>O<sub>7</sub>, *Phys. Rev. B* **87**, 184427 (2013).
- [39] P. Dalmas de Réotier, A. Maisuradze, and A. Yaouanc, Recent  $\mu$ SR studies of insulating rare-earth pyrochlore magnets, *J. Phys. Soc. Jpn.* **85**, 091010 (2016).
- [40] P. Dalmas de Réotier, A. Yaouanc, A. Maisuradze, A. Bertin, P. J. Baker, A. D. Hillier, and A. Forget, Slow spin tunneling in the paramagnetic phase of the pyrochlore Nd<sub>2</sub>Sn<sub>2</sub>O<sub>7</sub>, *Phys. Rev. B* **95**, 134420 (2017).
- [41] M. H. Dehn, J. K. Shenton, S. Holenstein, Q. N. Meier, D. J. Arseneau, D. L. Cortie, B. Hitti, A. C. Y. Fang, W. A. MacFarlane, R. M. L. McFadden, G. D. Morris, Z. Salman, H. Luetkens, M. Spaldin, and R. F. Kiefl, Observation of a charge-neutral muon-polaron complex in antiferromagnetic Cr<sub>2</sub>O<sub>3</sub>, [arXiv:1909.00416](https://arxiv.org/abs/1909.00416).
- [42] P. Villars and L. D. Calvert, *Pearson's Handbook of Crystallographic Data for Intermetallic Phases*, 2nd ed. (ASM International, Ohio, 1991).
- [43] T. Bernier, Y. Lejus, H. Tueta, and X. Collongues, Susceptibilité paramagnétique anisotrope de monocristaux d'oxydes Nd<sub>2</sub>O<sub>3</sub> et La<sub>x</sub>Nd<sub>2-x</sub>O<sub>3</sub>, *Mater. Res. Bull.* **8**, 261 (1973).
- [44] P. Caro, J. Derouet, L. Beaury, and E. Soulie, Interpretation of the optical absorption spectrum and of the paramagnetic susceptibility of neodymium A' type sesquioxide, *J. Chem. Phys.* **70**, 2542 (1979).
- [45] F. L. Pratt, A muon data analysis program for the Windows PC, *Physica B (Amsterdam)* **289**, 710 (2000).
- [46] S. R. Kretzman, R. F. Kiefl, D. R. Noakes, J. H. Brewer, and E. J. Ansaldo, Thermally activated muonium formation in Al<sub>2</sub>O<sub>3</sub> and BaF<sub>2</sub>, *Hyperfine Interact.* **32**, 521 (1986).
- [47] V. Storchak, J. H. Brewer, and G. D. Morris, Quantum transport of electronic polarons in sapphire, *Phys. Rev. B* **56**, 55 (1997).
- [48] I. Fan, K. H. Chow, B. Hitti, R. Scheuermann, A. I. Mansour, W. A. MacFarlane, B. E. Schultz, M. Egilmez, J. Jung, Y. G. Celebi, H. N. Bani-Salameh, B. R. Carroll, J. E. Vernon, and R. L. Lichti, Influence of photoexcitation on the diamagnetic muonium states in Ge studied via their precession signatures, *Phys. Rev. B* **78**, 153203 (2008).
- [49] R. C. Vilão, A. G. Marinopoulos, R. B. L. Vieira, A. Weidinger, H. V. Alberto, J. P. Duarte, J. M. Gil, J. S. Lord, and S. F. J. Cox, Hydrogen impurity in paratellurite  $\alpha$ -TeO<sub>2</sub>: Muon-spin rotation and *ab initio* studies, *Phys. Rev. B* **84**, 045201 (2011).
- [50] T. Prokscha, K. H. Chow, E. Stilp, A. Suter, H. Luetkens, E. Morenzoni, G. J. Nieuwenhuys, Z. Salman, and R. Scheuermann, Photo-induced persistent inversion of germanium in a 200-nm-deep surface region, *Sci. Rep.* **3**, 2569 (2013).
- [51] R. B. L. Vieira, R. C. Vilão, A. G. Marinopoulos, P. M. Gordo, J. A. Paixão, H. V. Alberto, J. M. Gil, A. Weidinger, R. L. Lichti, B. Baker, P. W. Mengyan, and J. S. Lord, Isolated hydrogen configurations in zirconia as seen by muon spin spectroscopy and *ab initio* calculations, *Phys. Rev. B* **94**, 115207 (2016).
- [52] H. V. Alberto, R. C. Vilão, R. B. L. Vieira, J. M. Gil, A. Weidinger, M. G. Sousa, J. P. Teixeira, A. F. da Cunha, J. P. Leitão, P. M. P. Salomé, P. A. Fernandes, T. Törndahl, T. Prokscha, A. Suter, and Z. Salman, Slow-muon study of quaternary solar-cell materials: Single layers and *p-n* junctions, *Phys. Rev. Mater.* **2**, 025402 (2018).
- [53] V. G. Storchak, D. G. Eshchenko, and J. H. Brewer, Formation and dynamics of muonium centres in semiconductors—a new approach, *J. Phys.: Condens. Matter* **16**, S4761 (2004).
- [54] J. D. Brewer, J. H. Brewer, G. D. Morris, D. G. Eshchenko, and V. G. Storchak, Electric-field-induced muonium formation in sapphire, *Physica B: Condens. Matter* **289**, 428 (2000).
- [55] E. L. Silva, A. G. Marinopoulos, R. C. Vilão, R. B. L. Vieira, H. V. Alberto, J. Piroto Duarte, and J. M. Gil, Hydrogen impurity in yttria: *Ab initio* and  $\mu$ SR perspectives, *Phys. Rev. B* **85**, 165211 (2012).
- [56] R. B. L. Vieira, R. C. Vilão, P. M. Gordo, A. G. Marinopoulos, H. V. Alberto, J. Piroto Duarte, J. M. Gil, A. Weidinger, and J. S. Lord, Muon-spin-rotation study of yttria-stabilized zirconia (ZrO<sub>2</sub>:Y): Evidence for muon and electron separate traps, *J. Phys.: Conf. Series* **551**, 012050 (2014).
- [57] J. R. Henderson, M. Muramoto, and J. B. Gruber, Spectrum of Nd<sup>3+</sup> in lanthanide oxide crystals, *J. Chem. Phys.* **46**, 2515 (1967).
- [58] B. H. Justice and E. F. Westrum, Thermophysical properties of the lanthanide oxides. I. Heat capacities, thermodynamic properties, and some energy levels of lanthanum (iii) and neodymium (iii) oxides from 5 to 350 K, *J. Phys. Chem.* **67**, 339 (1963).
- [59] R. C. Vilão, J. S. Lord, J. M. Gil, H. V. Alberto, and J. Piroto Duarte, Muonium in rare-earth sesquioxides, STFC ISIS Neutron and Muon Source (2012), <https://doi.org/10.5286/ISIS.E.24089275>.